A&A 521, L24 (2010)
DOI: 10.1051/0004-6361/201015099

Astronomy & Astrophysics
Special feature

Herschel/HIFI: first science highlights

Letter to the Editor

The origin of the [C II] emission in the S140 photon-dominated regions. New insights from HIFI⋆,⋆⋆

C. Dedes[1], M. Röllig[2], B. Mookerjea[3], Y. Okada[2], V. Ossenkopf[2,4], S. Bruderer[1], A. O. Benz[1], M. Melchior[5], C. Kramer[6], M. Gerin[7], R. Güsten[8], M. Akyilmaz[2], O. Berne[9], F. Boulanger[10], G. De Lange[4], L. Dubbeldam[4], K. France[11], A. Fuente[12], J. R. Goicoechea[13], A. Harris[14], R. Huisman[4], W. Jellema[4], C. Joblin[15,16], T. Klein[8], F. Le Petit[17], S. Lord[18], P. Martin[11], J. Martin-Pintado[13], D. A. Neufeld[19], S. Philipp[8], T. Phillips[20], P. Pilleri[15,16], J. R. Rizzo[13], M. Salez[21,7], R. Schieder[2], R. Simon[2], O. Siebertz[2], J. Stutzki[2], F. van der Tak[4,22], D. Teyssier[23], and H. Yorke[24]

(Affiliations are available on page 5 of the online edition)

Received 31 May 2010 / Accepted 28 July 2010

ABSTRACT

Using *Herschel's* HIFI instrument, we observe [C II] along a cut through S140, as well as high-J transitions of CO and HCO^+ at two positions on the cut, corresponding to the externally irradiated ionization front and the embedded massive star-forming core IRS1. The HIFI data were combined with available ground-based observations and modeled using the KOSMA-τ model for photon-dominated regions (PDRs). We derive the physical conditions in S140 and in particular the origin of [C II] emission around IRS1. We identify three distinct regions of [C II] emission from the cut, one close to the embedded source IRS1, one associated with the ionization front, and one further into the cloud. The line emission can be understood in terms of a clumpy model of PDRs. At the position of IRS1, we identify at least two distinct components contributing to the [C II] emission, one of them a small, hot component, which can possibly be identified with the irradiated outflow walls. This is consistent with the [C II] peak at IRS1 coinciding with shocked H_2 emission at the edges of the outflow cavity. We note that previously available observations of IRS1 can be reproduced well by a single-component KOSMA-τ model. Thus, it is HIFI's unprecedented spatial and spectral resolution, as well as its sensitivity that has allowed us to uncover an additional hot gas component in the S140 region.

Key words. ISM: structure – ISM: kinematics and dynamics – ISM: molecules – photon-dominated region (PDR) – submillimeter: general

1. Introduction

Massive star formation poses a challenge to the observer, since massive stars are formed predominantly in clustered environments and exhibit a number of entangled energetic phenomena in a small region. The S140 region displays evidence of several phenomena associated with (massive) star formation, such as outflows and strong UV irradiation from both internal and external heating sources creating photon-dominated regions (PDRs). Thus, S140 could also be used as a template for extragalactic star formation that is traced by strong fine structure lines stemming from PDRs.

At a distance of 910 pc, the B0V star HD 211880 ionizes the edge of the molecular cloud L1204, creating S140, a visible H II region and PDR (Crampton et al. 1974). The dense molecular cloud hosts a cluster of embedded massive young stellar objects (YSOs) only 75″ from the H II region (e.g., Beichman et al. 1979; Minchin et al. 1993). Both S140 and its surroundings have been extensively observed in molecular tracers (e.g., Minchin et al. 1993, 1995; van der Tak et al. 2000; Persson et al. 2009) and the fine structure lines, [C II] (Boreiko et al. 1990; White & Padman 1991; Li et al. 2002), [C I] (Minchin et al. 1994), and [O I] (Emery et al. 1996). An ionized component around IRS1 was detected by Hoare (2006) and Trinidad et al. (2007) at high resolution in the cm continuum observations. Spaans & van Dishoeck (1997) modeled S140 with a nearly edge-on geometry, a clumpy, inhomogeneous medium, and a radiation field of 150 Draine[1] units.

Two bi-polar outflows can be found in the S140 cloud (e.g., Weigelt et al. 2002; Preibisch et al. 2002). One is traced by observations of bow-shock-like features and H_2 knots, indicating hot, shocked gas, lined up northeast of IRS1 over several degrees, while the other, perpendicular to it, has been observed in CO.

In this paper, we describe and model the [C II], high-J CO and HCO^+ observations in the S140 region, observed as part of the WArm and Dense ISM key project (WADI, Ossenkopf et al., KPGT_vossenko_1) using the HIFI (de Graauw et al. 2010) instrument on the *Herschel* Space Observatory (Pilbratt et al. 2010). The goal of these studies it to investigate and compare the physical properties of the different gas phases in two regions of the S140 cloud, i.e. the star-forming region IRS1 and the ionization front (hereafter IF).

⋆ *Herschel* is an ESA space observatory with science instruments provided by European-led Principal Investigator consortia and with important participation from NASA.

⋆⋆ Acknowledgements and appendices (pages 5 to 7) are only available in electronic form at http://www.aanda.org

[1] In units of 2.7×10^{-3} erg cm^{-1} s^{-1} in the FUV wavelength range from 912 Å to 1110 Å.

2. Observations and analysis

2.1. HIFI observations

For this paper, two single-pointing, frequency-switching spectra in bands 1a, 4a, and 4b from the priority science phase and a [C II] OTF map from the science demonstration phase were analyzed. The single pointing data were taken towards S140-IRS1 at RA = $22^h19^m18.21^s$, Dec = 63°18′46.9″ (J2000) and towards a position in the IF at RA = $22^h19^m11.53^s$, Dec = 63°17′46.9″ (J2000). The fully sampled [C II] map is centered on RA = $22^h19^m18.88^s$, Dec = 63°18′52.9″ (J2000), has a length of 206″, and crosses the PDR region from the IF through IRS1 into the dense molecular cloud (Fig. 1, right). The data presented here were taken with the wide band spectrometer (WBS) at 1.1 MHz resolution. For the FSW data, the upper and lower sidebands were processed separately. All observational parameters are summarized in Table 1. The data reduction was performed using HIPE 3.0 (Ott et al. 2010). A forward efficiency of 96% and main beam efficiencies of 0.72, 0.74, 0.76, and 0.65 at 500, 950, 1112 and 1900 GHz, respectively (R. Moreno, priv. comm.), were used to convert the data to main beam temperatures T_{mb}.

2.2. Complementary data

We combined the HIFI data with observations of all CO isotopes in the 2–1 and 3–2 transitions, of ^{12}CO in the 4–3 and 7–6 transitions, HCO^+ and $H^{13}CO^+$ in the 3–2 and 4–3 transitions, and both fine structure lines of atomic carbon [CI], taken at the KOSMA 3m sub-mm telescope, the IRAM 30 m telescope, and the JCMT. For easy comparison of flux values, all data have been smoothed to the 80″ resolution of the KOSMA 345 GHz data. The procedure to derive appropriate scaling factors for the single-point observations with different beams, based on the spatial distribution measured in the SPIRE 250 μm and SCUBA 450 μm map, is described in detail in the Appendix.

2.3. PDR modeling

To model the physical parameters in IRS1 and the IF, we fit the data by the KOSMA-τ PDR code (Röllig et al. 2006). The PDR is represented by an ensemble of spherical clumps with a power-law clump-mass spectrum (Cubick et al. 2008). Details are summarized in Appendix B. Each clumpy PDR ensemble has five free parameters: the average density of the clumps in the ensemble, n_{ens}; the ensemble mass, M_{ens}; the UV field strength, χ, given in units of the Draine field; and the minimum and maximum mass of the clump ensemble, (M_{min}, M_{max}). We fit absolute line intensities, using the available ground-based observations and the HIFI lines of the CO isotopes, HCO^+, atomic, and ionized carbon. Simulated annealing (Ingber 1993) was used to find the optimum parameter combination. Our model ignores mutual shielding and illumination effects between different clumps and/or ensembles, i.e., optical depth effects are only considered within individual clumps.

3. Results

3.1. [CII] cut

Figure 1, left, shows the measured position-velocity diagram of the [C II] cut. We can distinguish three peaks. The first peak (IF-peak from now on), at around −1.2′, is located right at the edge of the rim of the IF as seen by White & Padman (1991) and represents the [C II] emission from the IF. A second, much broader

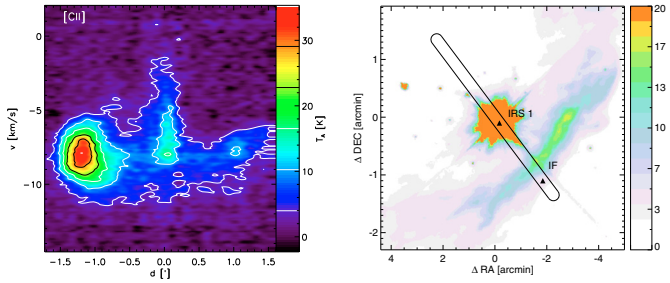

Fig. 1. *Left*: position-velocity diagram of the [C II] emission from the IF into the cloud, centered on RA = $22^h19^m18.88^s$, Dec = 63°18′52.9″ (J2000). IRS1 is at found at –7.5″. *Right*: IRAC 8 μm map of S140. Shown are the two positions at which individual HIFI measurements are taken as well as the location of the [C II] cut. HD 211880 is located to the left of the pv diagram, and to *the bottom right* of the cut in *the right panel*.

peak is found around 0′, in the vicinity of IRS1 (therefore called IRS1-peak). The third peak is located at 1′ into the dense cloud.

At the IF position, we see symmetric [C II] line profiles and no gradient in either line width or centroid velocity. We find indications neither of a pressure gradient nor an evaporation flow from the PDR surface. Looking at archival IRAC 8 μm data, the peak of the [C II] integrated intensity at the IF-peak is consistent with that of IRAC 8 μm, tracing the PAH and evaporating VSG emission.

The emission at the IRS1-peak is 10″ offset from the young stellar object IRS1 and coincident with the locations of the deeply embedded source Submm-2, which was first described by Minchin et al. (1995) and the strong H_2 knot #1 found by Preibisch et al. (2002). Compared to the *K*-band data of Weigelt et al. (2002), the [C II] peak is close to the edge of what they describe as the wall of the outflow cavity carved into the material by the jet. The strong [C II] emission seen here is probably created at this interface, by either irradiation of the outflow walls (e.g. Bruderer et al. 2009a,b) or shock interactions, as traced by the H_2 knots. The [C II] lines are very broad with a pronounced red wing tracing an outflow of ionized carbon, which is visible in Fig. 2 between −5 km s^{-1} and 0 km s^{-1}. A two-component Gaussian profile with components at −8 km s^{-1} and −5.5 km s^{-1} fits the observed [C II] line profile. Since the −5.5 km s^{-1} component of the [C II] emission is not observed in any of the other molecular tracers, it does not arise in the outflows, but may originate in the ionized medium. Between the two [C II] peaks, the [C II] emission drops significantly, indicating a spatial separation between the IF component and the component around IRS1. This drop in [C II] intensity between the IF-peak and IRS1-peak roughly coincides with a local minimum of the dust temperature, where the heating from neither the internal IRS1 source nor the external star (Lester et al. 1986) are efficient.

In the region where the third peak is seen in [C II], the SPIRE 250 μm map also shows a secondary peak (Juvela et al., priv. comm.), which appears to be a deeply embedded source. The [C II] line has pronounced wings, at a slightly higher velocity than in IRS1. This might be indicative of a separate outflow or material shocked by the outflow from IRS1.

Several spectra were taken with HIFI at the IRS1 and IF position. Overlay of those spectra of different tracers shows that with the exception of [C II] all the molecular lines at IRS1 have similar line shapes (Fig. 2). The [C II] line displays a strong red wing, which was also undetected in the previous coarser spatial resolution observations by Boreiko et al. (1990). The centroid velocity, v_{cen}, of all the molecular lines ranges from −6.8 to −7.4 km s^{-1}

Table 1. Summary of the HIFI observations used and basic results.

Transition	$\nu_{\rm line}$	HPBW	Mode[1]	S140-IRS1					S140-IF				
				$t_{\rm source}$	rms[2]	$\int T{\rm d}v$	$v_{\rm lsr}$	Δv	$t_{\rm source}$	rms[2]	$\int T{\rm d}v$	$v_{\rm lsr}$	Δv
	[GHz]	$''$		[s]	[K]	(K km s^{-1})	(km s^{-1})	(km s^{-1})	[s]	[K]	(K km s^{-1})	(km s^{-1})	(km s^{-1})
CII	1900.537	12	OTF	12	0.9	59.63 (0.99)	–7.26 (0.05)	6.82 (0.15)	12	0.9	96.91 (0.60)	–8.00 (9.2e-03)	3.05 (0.02)
^{13}CO(5–4)	550.926	43	FSW	480	0.02	85.74 (2.48)	–7.24 (0.06)	4.02 (0.14)	240	0.03	4.56 (0.04)	–7.89 (0.01)	2.85 (0.03)
C^{18}O(5–4)	548.831	43	FSW	480	0.02	17.29 (0.07)	–7.24 (5.7e-03)	2.98 (0.01)	240	0.03	0.47 (0.03)	–7.66 (0.08)	2.21 (0.17)
HCO$^+$(6–5)	535.062	43	FSW	480	0.02	38.96 (4.90)	–6.77 (0.23)	3.75 (0.57)	240	0.16	0.67 (0.28)	–7.52 (0.74)	3.48 (1.63)
C^{18}O(9–8)	987.56	23	FSW	66	0.1	2.60 (0.07)	–7.03 (0.04)	2.92 (0.09)	…	…	…	…	…
^{13}CO(10–9)	1101.35	20	FSW	156	0.15	23.41 (0.73)	–6.99 (0.06)	3.93 (0.15)	…	…	…	…	…

Notes. [(1)] OTF = On-The-Fly, FSW = frequency-switch, OFF position = 22$^{\rm h}$18$^{\rm m}$37.01$^{\rm s}$, 63°14′17.9″ . [(2)] At a velocity resolution of Δv = 0.7 km s^{-1}.

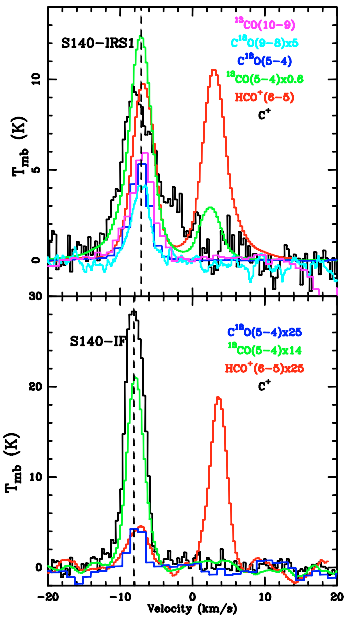

Fig. 2. HIFI spectra at IRS1 and the IF. The additional ghost line at 4 km s^{-1} in the HCO$^+$(6–5) and ^{13}CO(5–4) data is an artifact produced by the FSW deconvolution of the two lines, close in IF frequency but stemming from different receiver sidebands. Some lines are scaled for a better comparison. The two dashed lines represent the $v_{\rm lsr}$ at −7.1 km s^{-1} (IRS1) and −8 km s^{-1} (IF).

and agrees well with a source velocity of −7.1 km s^{-1} derived from previous observations (e.g., van der Tak et al. 2000; Persson et al. 2009). Although somewhat fainter in intensity (particularly in the case of HCO$^+$ 6–5), several of the molecular lines are still detected at the IF position. The line widths at the IF position are up to a factor of two narrower than the widths at the position of IRS1. At the IF position, the centroid velocities fall between −7.5 to −8.0 km s^{-1}, corresponding to a slight blue shift compared to the velocities at the IRS1 position. Detailed discussion of the [C II] line profiles will be taken up in a later paper by Mookerjea et al. (in prep.).

3.2. PDR model in IRS1

Since the PDR region arising from the irradiated outflow walls is illuminated from both the outside by the B0V star HD 211880 and the inside by the cluster of YSOs around IRS1, we assume a two component fit with a hot component originating at IRS1 with strong FUV illumination, but only a small fraction of the total mass, and a cooler component that provides the bulk of the material. Owing to the much coarser resolution of the available hydrogen and carbon radio recombination lines (Smirnov et al. 1995; Wyrowski et al. 1997), it is difficult to ascertain the

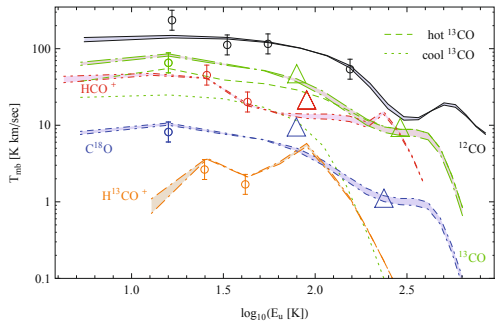

Fig. 3. Clumpy PDR model fit to the observed CO and HCO$^+$ line integrated intensities in IRS1, shown as a function of the upper level energy. HIFI measurements are depicted as open triangles, complementary data points as open circles. The range of model intensities spanned by the total mass range of 54–250 $M_\odot$ for the cool component is shown as shaded area for the J-lines.

Table 2. The parameters for the two ensembles in the PDR model in IRS1.

$\langle n_{\rm ens}\rangle$ (cm^{-3})	$M_{\rm ens}$ ($M_\odot$)	χ (Draine)	$[M_{\rm min}, M_{\rm max}]$ ($M_\odot$)	N[1]	$f_{\rm V}$	f_A[2]
Hot:						
1.8×10^6	14	2.3×10^5	[0.008, 7]	151	0.42–0.73	1.3
Cool:						
1.3×10^6	54–250	27	[0.008, 27]	413–1913	0.07–0.34	0.6–2.6

Notes. [(1)] Number of all clumps; [(2)] assuming hot clumps are situated approximately 7″ away from IRS1; $f_{\rm V}$ volume filling factor within a shell with $R_{\rm V,inner}$ = 5″ and $R_{\rm V,outer}$ = 11–13″; $f_{\rm A}$ area filling factor with $R_{\rm A}$ = 7″ for the hot component. For the cold component, $R_{\rm V,inner}$ = 11–13″, $R_{\rm V,outer}$ = 40″, and $R_{\rm A}$ = 40″.

fraction (if any) of [C II] emission contributed by the ionized gas associated with IRS1. Based on the Gaussian decomposition described in Sect. 3.1, the [C II] intensity from the PDR must fall between the 60 K km s^{-1} of the total integrated line and the 37 K km s^{-1} of the −8 km s^{-1} component only. We consequently obtain two different limiting fits that differ mainly in terms of the mass of the cool component between 54 and 250 $M_\odot$. The best fit result is shown in Fig. 3. The corresponding model parameters for both components can be found in Table 2. Figure 3 also indicates the contributions of the two components to the emission.

The reduced χ^2 of the fit is 2.4. We applied a generic 30% error to all data points. The model slightly underestimates the mid- J lines of the CO isotopologues and of HCO$^+$. This is the energetic region where neither the cool nor the hot component are very bright, so that this may hint towards a third intermediate component. However, the available data do not allow us to reliably derive parameters of a third component. To see the modeled FUV flux of the hot component, the clumps have to be at a

Table 3. PDR model fit to the observed atomic fine structure line integrated intensities in IRS1.

Species	Total (K km s^{-1})	hot (K km s^{-1})	Cool (K km s^{-1})	Obs. (K km s^{-1})
[C II]	19.3–21.9	16.5	2.8–5.4	37.
[C I](1–0)	9.7–11.0	1.5	8.2–9.5	11.4
[C I](2–1)	6.9–8.5	1.7	5.2–6.8	20.5

Notes. Shown are the ranges spanned by the two fits.

distance of 7″ from IRS1. At this distance, an area filling factor on a spherical shell of 1.3 is obtained, i.e. the hot component shields the cool ensemble from most of the FUV flux. To obtain reasonable values of volume filling factors, i.e. $0.42 \leq f_V \leq 0.73$, the inner and outer radii of the shell have to be roughly equivalent to 5″ and 11–13″, respectively. While at the larger radii, the FUV flux seen by the hot component would be somewhat lower than predicted by our model, this discrepancy is still small compared to the uncertainties in the line estimates and thus the model parameters.

The model parameters of the cool ensemble are particularly interesting. The FUV field is lower than expected from the externally illuminating star HD 211880. This suggests that the prominent edge-on PDR at the IF blocks the FUV radiation.

3.3. PDR model in the IF

For the IF position, we are not yet able to provide a full model fit to the data because of the lower numbers of detected lines. We can, however, derive some qualitative conclusions. The mid- and high-J lines of CO and HCO^+ can only be explained by a hot gas component with densities on the order of 10^6 cm^{-3} and a local FUV intensity on the order of 10^5 Draine units. The external radiation from HD 211880 cannot provide more than a few thousand Draine units. An additional, so far unknown UV source seems to be present. The total gas mass in the beam at the IF is on the order of 10 $M_\odot$.

4. Discussion and conclusions

About 90% of the [C II] emission around IRS1 stems from the hot component near the embedded IR sources. A different heating mechanism accounts for the [CII] from the emission in the ionizing front. This is reflected in our choice of two separate models for the two regions.

Previous models of PDR emission in S140 (Spaans & van Dishoeck 1997) described the S140 region as an inhomogeneous medium with $\langle n_H \rangle = 7 \times 10^3$ cm^{-3}, a filling factor of 30%, and clumps of 0.04 pc size. The radiation field, χ, of 150 Draine units that they derived is much lower than the one derived in this work. These authors included the IRS1 cluster as an embedded heating source in their model, yet did not distinguish between the two regions of [C II] emission – the IRS1 region and the IF. They were also unable to include high-J CO lines, which are important tracers of the hot gas. In our two component approach, the high-J CO lines on the one hand tell us how strong the hot ensemble has to be illuminated by the FUV and they determine how the total mass is distributed between hot and cool component. High-J CO lines will be especially valuable since they, in the context of PDR models, can only be produced by the very high FUV fields, while lower-J lines have always more mixed origins, hence pose weaker constraints on the multi-component model. With the exception of the high-J ^{13}CO(10–9) and C^{18}O(9–8) lines, most other data points can be explained by far more moderate FUV fields.

When repeating our calculations using only pre-HIFI data, we reproduce the parameters obtained in previous models (e.g., Spaans & van Dishoeck 1997; Köster 1998). It becomes apparent that only HIFI data can reveal additional components deep inside the cloud. The low mass of the hot component and the weak FUV field of the cool component suggests that only a small fraction of the material is affected by the full FUV field, supposedly where the outflows created cavity walls at the edge of the ambient material. The bulk of the material is effectively shielded from the FUV photons.

At the IF, our first qualitative results hint at a so-far unknown heating source and a two component density structure. A full PDR-model at this position (Röllig et al., in prep.) should provide additional insight into the properties of the material at the IF.

HIFI's high spectral resolution observations allow us to identify the general velocity fields of the molecular and ionized gas around IRS1 and trace the dynamics of the region, such as the blue outflow emission associated with the SPIRE-peak. This is possibly due to another, still deeply embedded object, which is driving its own outflow.

References

Beichman, C. A., Becklin, E. E., & Wynn-Williams, C. G. 1979, ApJ, 232, L47
Boreiko, R. T., Betz, A. L., & Zmuidzinas, J. 1990, ApJ, 353, 181
Bruderer, S., Benz, A. O., Bourke, T. L., & Doty, S. D. 2009a, A&A, 503, L13
Bruderer, S., Benz, A. O., Doty, S. D., van Dishoeck, E. F., & Bourke, T. L. 2009b, ApJ, 700, 872
Crampton, D., & Fisher, W. A. 1974, Publ. Dom. Astrophys. Obs., 14 , 283
Cubick, M., Stutzki, J., Ossenkopf, V., Kramer, C., & Röllig, M. 2008, A&A, 488, 623
de Graauw, Th., Helmich, F. P., Phillips, T. G., et al. 2010, A&A, 518, L6
Emery, R., Aannestad, P., Minchin, N., et al. 1996, 315, 285
Heithausen, A., Bensch, F., Stutzki, J., Falgarone, E., & Panis, J. F. 1998, A&A, 331, L65
Hoare, M. G. 2006, ApJ, 649, 856
Ingber, L. 1993, Simulated Annealing: Practice versus Theory, Mathematical Computer Modelling, 18, 29
Kaufman, M., Wolfire, M. G., & Hollenbach, D. J. 2006, ApJ, 644, 283
Köster, B. 1998, Ph.D. Thesis, Univ. Cologne, Germany
Kramer, C., Stutzki, J., Rohrig, R., et al. 1998, A&A, 329, 249
Kramer, C., Mookerjea, B., Bayet, E., et al. 2005, A&A, 441, 961
Lester, D. F., Harvey, P. M., Joy, M., & Ellis, H. B. Jr. 1986, ApJ, 309, 80
Li, W., Evans II, N. J., Jaffe, D. T., van Dishoeck, E. F., & Thi, W. 2002, ApJ, 568, 242
Minchin, N. R., White, G. J., & Padman, R. 1993, A&A, 277, 595
Minchin, N. R., White, G. J., Stutzki, J., & Krause, D. 1994, A&A, 291, 250
Minchin, N. R., Ward-Thompson, D., & White, G. J. 1995, A&A, 298, 894
Ott, S. 2010, in Astronomical Data Analysis Software and Systems XIX, ed. Y. Mizumoto, K.-I. Morita, & M. Ohishi, ASP Conf. Ser., in press
Persson, C. M., Olberg, M., Hjalmarson, Å., et al. 2009, A&A, 494, 637
Pilbratt, G. L., Riedinger, J. R., Passvogel, T., et al. 2010, A&A, 518, L1
Preibisch, T., & Smith, M. D. 2002, A&A, 383, 540
Röllig, M., Ossenkopf, V., Jeyakumar, S., Stutzki, J., & Sternberg, A. 2006, A&A, 451, 917
Röllig, M., Abel, N. P., Bell, T., et al. 2007, A&A, 467, 187
Smirnov, G. T., Sorochenko, R. L., & Walmsley, C. M. 1995, A&A, 300, 923
Spaans, M., & van Dishoeck, E. F. 1997, A&A, 323, 953
Trinidad, M. A., Torrelles, J. M., Rodriguez, L. F., & Curiel, S. 2007, AJ, 134, 1870
van der Tak, F. F. S., van Dishoeck, E. F., Evans II, N. J., & Blake, G. A. 2000, ApJ, 537, 283
Viti, S., Hartquist, T. W., & Myers, P. C. 2006, Ap&SS, 302, 109
Weigelt, G., Balega, Y. Y., Preibisch, T., Schertl, D., & Smith, M. D. 2002, A&A, 381, 905
White, G. J., & Padman, R. 1991, Nature, 354, 511
Woodall, J., Agúndez, M., Markwick-Kemper, A. J., & Millar, T. J. 2007, A&A 466, 1197
Wyrowski, F., Walmsley, C. M., Natta, A., & Tielens, A. G. G. M. 1997, A&A, 324, 1135

Acknowledgements. HIFI has been designed and built by a consortium of institutes and university departments from across Europe, Canada and the United States under the leadership of SRON Netherlands Institute for Space Research, Groningen, The Netherlands and with major contributions from Germany, France and the US. Consortium members are: Canada: CSA, U.Waterloo; France: CESR, LAB, LERMA, IRAM; Germany: KOSMA, MPIfR, MPS; Ireland, NUI Maynooth; Italy: ASI, IFSI-INAF, Osservatorio Astrofisico di Arcetri- INAF; Netherlands: SRON, TUD; Poland: CAMK, CBK; Spain: Observatorio Astronomico Nacional (IGN), Centro de Astrobiologia (CSIC-INTA). Sweden: Chalmers University of Technology – MC2, RSS & GARD; Onsala Space Observatory; Swedish National Space Board, Stockholm University – Stockholm Observatory; Switzerland: ETH Zurich, FHNW; USA: Caltech, JPL, NHSC. The work on star formation at ETH Zurich is partially funded by the Swiss National Science Foundation (grant nr. 200020-113556). This program is made possible thanks to the Swiss HIFI guaranteed time program. This work was supported by the German *Deutsche Forschungsgemeinschaft, DFG* project number Os 177/1–1. We thank the members of the *Herschel* key project "Galactic Cold Cores: A *Herschel* survey of the source populations revealed by Planck" lead by M. Juvela (KPOT_mjuvela_1) for providing us with the results of the SPIRE 250 μm mapping and fruitful discussions. We would also like to acknowledge the use of the JCMT CO(3–2) archival data (PI M. Thompson, M08BU15). A portion of this research was performed at the Jet Propulsion Laboratory, California Institute of Technology, under contract with the National Aeronautics and Space administration. We would like to thank an anonymous referee for constructive comments.

[1] Institute for Astronomy, ETH Zürich, 8093 Zürich, Switzerland
[2] I. Physikalisches Institut der Universität zu Köln, Zülpicher Straße 77, 50937 Köln, Germany
e-mail: carolin.dedes@astro.phys.ethz.ch
[3] Tata Institute of Fundamental Research (TIFR), Homi Bhabha Road, Mumbai 400005, India
[4] SRON Netherlands Institute for Space Research, PO Box 800, 9700 AV Groningen, The Netherlands
[5] Institut für 4D-Technologien, FHNW, 5210 Windisch, Switzerland
[6] Instituto de Radio Astronomía Milimétrica (IRAM), Avenida Divina Pastora 7, Local 20, 18012 Granada, Spain
[7] LERMA, Observatoire de Paris, 61 Av. de l'Observatoire, 75014 Paris, France
[8] Max-Planck-Institut für Radioastronomie, Auf dem Hügel 69, 53121, Bonn, Germany
[9] Leiden Observatory, Universiteit Leiden, PO Box 9513, 2300 RA Leiden, The Netherlands
[10] Institut d'Astrophysique Spatiale, Université Paris-Sud, Bât. 121, 91405 Orsay Cedex, France
[11] Department of Astronomy and Astrophysics, University of Toronto, 60 St. George Street, Toronto, ON M5S 3H8, Canada
[12] Observatorio Astronómico Nacional (OAN), Apdo. 112, 28803 Alcalá de Henares (Madrid), Spain
[13] Centro de Astrobiología (INTA-CSIC), Ctra de Torrejón a Ajalvir, km 4, 28850 Torrejón de Ardoz, Madrid, Spain
[14] Astronomy Department, University of Maryland, College Park, MD 20742, USA
[15] Université de Toulouse, UPS, CESR, 9 avenue du colonel Roche, 31062 Toulouse Cedex 4, France
[16] CNRS, UMR 5187, 31028 Toulouse, France
[17] Observatoire de Paris, LUTH and Université Denis Diderot, Place J. Janssen, 92190 Meudon, France
[18] IPAC/Caltech, MS 100-22, Pasadena, CA 91125, USA
[19] Department of Physics and Astronomy, Johns Hopkins University, 3400 North Charles Street, Baltimore, MD 21218, USA
[20] California Institute of Technology, 320-47, Pasadena, CA 91125-4700, USA
[21] Laboratoire d'Études du Rayonnement et de la Matière en Astrophysique, UMR 8112 CNRS/INSU, OP, ENS, UPMC, UCP, Paris, France
[22] Kapteyn Astronomical Institute, University of Groningen, PO box 800, 9700 AV Groningen, The Netherlands
[23] European Space Astronomy Centre, Urb. Villafranca del Castillo, PO Box 50727, 28080 Madrid, Spain
[24] Jet Propulsion Laboratory, 4800 Oak Grove Drive, MC 302-231, Pasadena, CA 91109, USA

Table A.1. The scaling factors between the different beam size observations, which should be multiplied to the line intensity to estimate the one in a 80″ beam.

IRS1	
beam size (″)	scaling factor
19.7	0.40
42.0	0.57
43.0	0.55
55.0	0.70
80.0	1.00

Appendix A: Comparison of line profiles taken with different beams

The different lines discussed here were measured at various telescopes and at different frequencies, so that they all represent somewhat different spatial resolutions. To allow a comparison in terms of a physical interpretation, they have to be translated to a common resolution, so that they stem from the same area on the sky. As a reference, we use 80″, the resolution of the KOSMA observations in the 3–2 transition of the CO isotopes. In principle, all data taken at a finer resolution can be resampled to this beam if the mapped area is large enough.

Unfortunately, most HIFI observations were only single-point observations, not full maps, so that such a convolution is impossible. To derive scaling factors that describe the translation between the measured intensities and the intensity that would be obtained in an 80″ beam, we have to assume a source geometry of the emission. Instead of using any analytic geometry, we use the actually measured distribution of warm dust seen in the sub-mm. By assuming that the spatial distribution of all PDR tracers roughly follows the warm dust, we derive scaling factors for the line intensities at different beam widths, by convolving the sub-mm continuum map with the different beam sizes and picking ratios between the convolved intensities at the measured positions. As a continuum map at IRS1, we used the combination of the SPIRE 250 μm (18″ beam size[2]) and SCUBA 450 μm image (8″ beam size, Holland et al. 1999), because IRS1 is saturated in SPIRE 250 μm, whereas the observed area of SCUBA 450 μm is too small to make a convolution map with the beam size of 80″. We regrid the SCUBA 450 μm image to the same grid as SPIRE 250 μm, determine the scaling factor between the SCUBA 450 μm and the SPIRE 250 μm maps from the overlapping area, and replace the saturated pixels of SPIRE 250 μm with the scaled SCUBA data. As this combination implies some arbitrariness, we tested four different approaches. We derive the scaling factor in a least squares fit using either (1) all the valid overlapping pixels or (2) only overlapping pixels with SPIRE 250 μm >100 Jy/beam. When replacing SPIRE pixels, we replace either (1) only saturated pixels, or (2) the full square area (5 × 5 pixels) containing all saturated pixels. The combination of these provide 4 different beam scaling factors, which are consistent to within 3%. Taking the average of these 4 values, we derive the final factors as shown in Table A.1. A direct convolution to 80″ was possible for the ground-based maps that were observed with a smaller beam, such as the JCMT CO(3–2) map. All the resulting intensities are summarized in Table A.2.

[2] http://herschel.esac.esa.int/Docs/SPIRE/html/spire_om.html

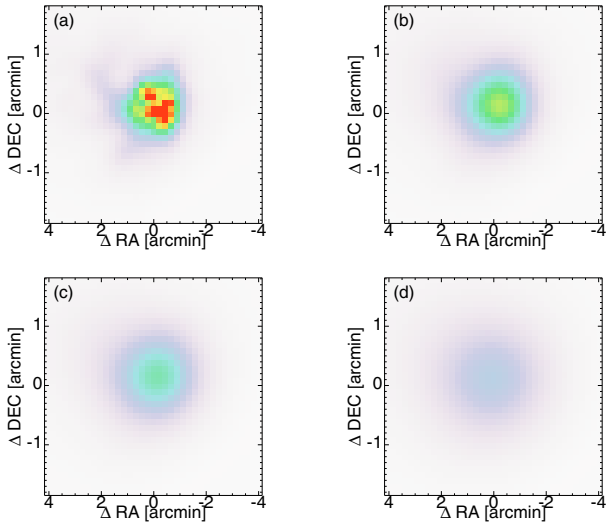

Fig. A.1. a) The spatial distribution of warm dust obtained by combining the SPIRE 250μm map with the SCUBA 450 μm map (see text). The HIFI beam is assumed to "see" convolved images at beam sizes of **b)** 42″, **c)** 55″, and **d)** 80″. The color scale is common to all the figures. The coordinates are relative to the position of IRS1. Thus, the flux ratios at (0, 0) in these images are the values in Table A.1.

Table A.2. List of the complementary data.

Tracer	IRS1 (K kms^{-1})	Beam (″)	Telescope
CO(2–1)	(130)	130	KOSMA[a]
^{13}CO(2–1)	(36.1)	130	KOSMA[a]
C^{18}O(2–1)	8.2	11.2	IRAM[b]
CO(3–2)	112.2	11.4	JCMT[c]
^{13}CO(3–2)	75.5	80	KOSMA[a]
CO(4–3)	115.5	57	KOSMA[d]
CO(7–6)	54.0	42	KOSMA[d]
CI($^3P_1$ –^{3} P_0)	11.4	55	KOSMA[d]
CI($^3P_2$ –^{3} P_1)	20.5	42	KOSMA[d]
HCO$^+$(3–2)	45.2	19.7	JCMT[e]
H^{13}CO$^+$(3–2)	(1.46)	130	KOSMA[f]
HCO$^+$(4–3)	20.12	13.2	JCMT[e]
H^{13}CO$^+$(4–3)	1.69	80	KOSMA[f]

Notes. All fluxes have been scaled to 80″ beam size. Values in brackets were not included in the fit.
[(a)] D. Bremaud, Diplomarbeit, ETH, [(b)] Kramer et al. (1998) [(c)] M. Thompson, JCMT archive, [(d)] S. Heyminck, priv. comm., [(e)] S. Bruderer, priv. comm., [(f)] E. Buenzli, Diplomarbeit ETH.

Appendix B: The clumpy PDR model

To model the far-infrared line emission from S140, we used a superposition of spherical clumps described by the KOSMA-τ PDR model (Röllig et al. 2006) that represent an ensemble of clumps with a fixed size-spectrum (Cubick et al. 2008). The KOSMA-τ PDR model simulates a spherical cloud with a radial density profile given by

$$n(r) = n_s \begin{cases} c^\delta & \text{for } r \le R/c \\ (r/R)^{-\delta} & \text{for } R/c < r \le R \\ 0 & \text{for } r > R. \end{cases} \quad \text{(B.1)}$$

The constant c determines the dynamic range that is covered by the power-law density decay. The spectrum of PDR clumps is characterized by the clump mass spectrum

$$\frac{\mathrm{d}N}{\mathrm{d}M} = aM^{-\alpha}, \tag{B.2}$$

where the factor a is determined by the total mass of clumps within the beam, M_{ens}, and the mass-size relation

$$M = CR^{\gamma}, \tag{B.3}$$

which implicitly defines the surface density of the individual clumps n_{s}. The factor C is determined by the average ensemble density n_{ens}. Guided by the clump-decomposition results from Heithausen et al. (1998), we fix the parameters of the spectrum to be $\alpha = 1.8$, $\gamma = 2.3$, $\delta = 1.5$, and $c = 5$. The boundaries of the clump size distribution M_{min} and M_{max} are used as free parameters with the constraint that the maximum clump mass cannot exceed half of the mass of the total ensemble.

Every individual clump is treated as a spherically symmetric configuration illuminated by an isotropic external UV radiation field, specified in terms of the average interstellar radiation field, $\chi_0 = 2.7 \times 10^{-3}$ erg cm^{-2} s^{-1} in Draine units, and cosmic rays producing an average ionization rate, $\zeta_{\mathrm{CR}} = 5 \times 10^{-17}$ s^{-1}. The internal velocity dispersion of molecules within the clumps is fixed to 1 km s^{-1}. The model computes the stationary chemical and temperature structure by solving the coupled detailed balance of heating, line and continuum cooling, and the chemical network using the UMIST data base of reaction rates (Woodall et al. 2007) expanded by separate entries for the ^{13}C chemistry (see Röllig et al. 2007, for details). The chemical network currently does not include ^{18}O, so that C^{18}O predictions can only be obtained by scaling the ^{13}CO values ignoring fractionation between the two species. As this ignores the different self-shielding of ^{13}CO and C^{18}O, the model results for C^{18}O are less reliable than for the other lines.

In the superposition of clumps, the line emission from the different clumps is simply added assuming that the velocity dispersion between the clumps is large enough, so that they do not shield each other in position-velocity space. This is valid for most species, except for the [O I] emission, which is optically very thick ($\tau \gtrsim 100$), so that the lines are much broader than the velocity distribution. Therefore, the model is unable to provide any reliable estimate of the [O I] intensities. For the continuum extinction of the UV radiation, the situation is different. There, mutual shading of the clouds is relevant, leading to the concept of different clump ensembles that "see" different UV fields if the average ensemble extinction exceeds an A_{V} of about unity.

The parameters of the clump mass spectrum imply that most of the mass is actually contained in the largest clumps that also have the maximum column density or A_{V}, respectively. The dependence of A_{V} and clump size on clump mass is given by

$$R = 5.3 \times 10^{18} \left(\frac{M[M_{\odot}]}{n[\mathrm{cm}^{-3}]} \right)^{\frac{1}{3}} \tag{B.4}$$

and

$$A_{\mathrm{V}} = 1.6018 \times 10^{21} n[\mathrm{cm}^{-3}] R[\mathrm{cm}]. \tag{B.5}$$

In terms of the total clump surface or the total solid angle of the different clumps, we find about equal contributions from each logarithmic mass bin in the ensemble (Eq. (16) in Cubick et al. 2008). Consequently, we find a non-trivial dependence of the intensity in the different HIFI lines on the clump mass. Figures 3 and 5 from Cubick et al. (2008) show that the [CII] emission is dominated by the largest clumps, while the high-J CO lines are dominated by the smallest clumps. A complex, non-monotonic behavior is observed for the lines from atomic oxygen and mid- to low-J CO isotopes.

As the clump spectrum is purely observationally based, it has no direct relation to a stability criterion. We indeed find that both the most massive clumps are unstable to gravitational collapse and that the smallest clumps will be dispersed on the timescale of a few million years. Therefore, the spectrum can only be considered as a snapshot of interstellar turbulence that reflects the density structure over a timescale of 10^6–10^7 years. The assumption of a steady-state chemistry and energy-balance is therefore only applicable if all rates are higher. This holds for the dense clumps in the S140 model fit with densities above 10^4 cm^{-3}, but for lower densities, an explicitly time-dependent modeling would be required (Viti et al. 2006).